

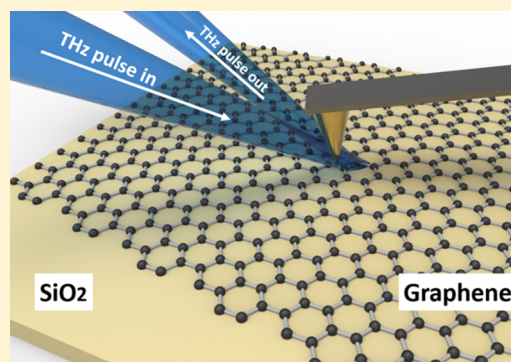
Terahertz Nanoimaging of Graphene

Jiawei Zhang,^{†,‡,§} Xinzhong Chen,^{†,‡} Scott Mills,[†] Thomas Ciavatti,[†] Ziheng Yao,[†] Ryan Mescall,[†] Hai Hu,[§] Vyacheslav Semenenko,^{||} Zhe Fei,[⊥] Hua Li,[#] Vasili Perebeinos,^{||} Hu Tao,[○] Qing Dai,[§] Xu Du,^{†,§} and Mengkun Liu^{*,†}[†]Department of Physics, Stony Brook University, Stony Brook, New York 11794, United States[§]Nanophotonics Research Division, CAS Center for Excellence in Nanoscience, National Center for Nanoscience and Technology, Beijing 100190, China^{||}Skolkovo Institute of Science and Technology, Skolkovo, Moscow Region 143026, Russia[⊥]Department of Physics and Astronomy, Iowa State University, Ames, Iowa 50011, United States[#]Key Laboratory of Terahertz Solid State Technology, Shanghai Institute of Microsystem and Information Technology, Chinese Academy of Sciences, Shanghai 200050, China[○]State Key Laboratory of Transducer Technology, Shanghai Institute of Microsystem and Information Technology, Chinese Academy of Sciences, Shanghai 200050, China

Supporting Information

ABSTRACT: Accessing the nonradiative near-field electromagnetic interactions with high in-plane momentum (q) is the key to achieve super resolution imaging far beyond the diffraction limit. At far-infrared and terahertz (THz) wavelengths (e.g., $300\ \mu\text{m} = 1\ \text{terahertz} = 4\ \text{meV}$), the study of high q response and nanoscale near-field imaging is still a nascent research field. In this work, we report on THz nanoimaging of exfoliated single and multilayer graphene flakes by using a state-of-the-art scattering-type near-field optical microscope (s-SNOM). We experimentally demonstrated that the single layer graphene is close to a perfect near-field reflector at ambient environment, comparable to that of the noble metal films at the same frequency range. Further modeling and analysis considering the nonlocal graphene conductivity indicate that the high near-field reflectivity of graphene is a rather universal behavior: graphene operates as a perfect high- q reflector at room temperature. Our work uncovers the unique high- q THz response of graphene, which is essential for future applications of graphene in nano-optics or tip-enhanced technologies.

KEYWORDS: terahertz s-SNOM, near field imaging, nanoimaging, graphene, high momentum, nonlocal conductivity



Terahertz technology, the application of electromagnetic wave ranging from 0.1 to 10 THz ($\sim 3000\ \mu\text{m}$ to $\sim 30\ \mu\text{m}$) has demonstrated a great potential in material identification,¹ security screening,² and high-speed communications.³ In particular, THz imaging promises to be a unique and powerful technique for low energy and spatially resolved spectroscopy of biological^{4–6} and solid state materials.^{7,8} Conventional THz “far-field” imaging with q close to zero, however, only reaches submillimeter resolution due to the diffraction limit.^{7,9} Therefore, to image small objects such as biological molecules or nanoparticles with sizes far below micrometer sizes, a near-field THz system is highly demanded.^{10–13}

Graphene has been demonstrated to possess fascinating optical properties in the THz frequency range, primarily due to its unique Dirac band structure, high carrier mobility, and good electrostatic tunability.^{14–18} In the far-field, graphene and graphene devices can be used as THz modulators with a tunable absorption ranging from below 10% to above 90%.¹⁹ In

the near-field, graphene carries plasmon polaritons at IR and THz ranges,^{20–24} promising on-chip optoelectronic applications at the nanoscale. Previous studies have revealed that the number of graphene layer has a dramatic impact on the near-field response in the mid-infrared regime.²⁵ In this work, using a THz scattering-type scanning near-field optical microscope, we show that, in contrast to the low THz reflection in the far-field measurements,²⁶ graphene can be regarded as an almost perfect THz reflector down to a monolayer at sufficiently high in-plane momentum q ($>10^5\ \text{cm}^{-1}$). Such strong near-field THz reflection is directly associated with graphene’s large in-plane conductivity probed by high q optics.

The schematic of our THz s-SNOM is shown in Figure 1a. This setup is based on a commercial atomic force microscope (AFM) with ample optical access from the front top (NTEGRA-IR, NT-MDT). Ultrafast THz pulses (0.2–2

Received: February 12, 2018

Published: June 21, 2018

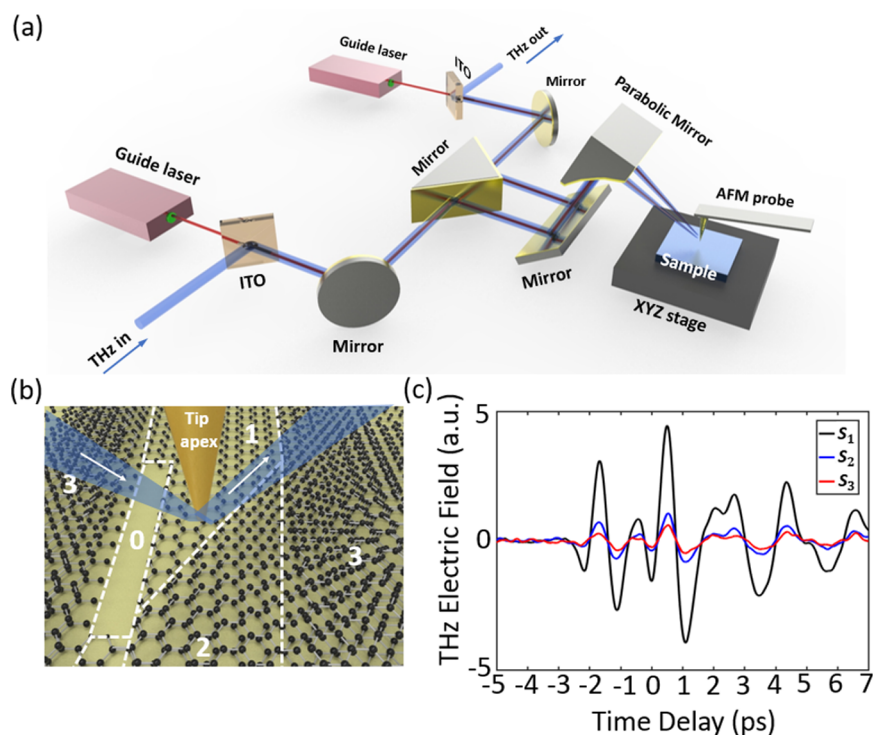


Figure 1. (a) Schematic of the THz *s*-SNOM setup. The blue (red) beam represents THz (guide) beam path. The THz PCA emitter, receiver, the 800 nm gate beam, and the delay stage are omitted from the schematic. The two visible guide lasers are used to trace the THz beam path for THz-tip alignment. (b) Schematic of graphene on SiO₂ with various numbers of layers. The region of the bare SiO₂ area is marked as 0. The number of layers is represented by the numbers on top of the schematics. (c) Demodulated time domain THz signal on a gold film at first (*S*₁), second (*S*₂), and third (*S*₃) harmonics of tip-tapping frequency.

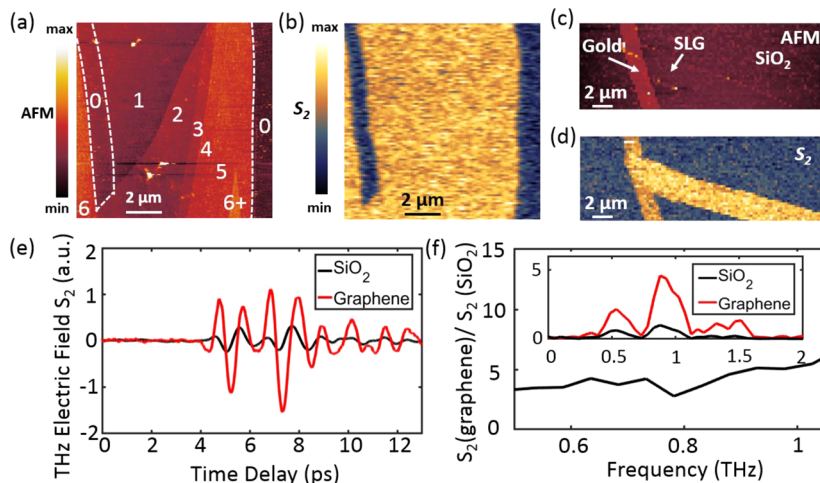


Figure 2. (a, b) AFM topography and THz near-field (*S*₂) mapping of graphene on SiO₂, respectively. The numbers of graphene layers are marked in (a), with bare SiO₂ marked as 0. (c, d) AFM and THz near-field (*S*₂) images of a SLG with a gold electrode. The near-field signal in graphene is comparable to that on the thin gold films. (e) Near field THz-TDS signal of SiO₂ (black) and graphene (red). (f) Normalized graphene THz near-field spectrum (to SiO₂). The inset shows a Fast Fourier Transform (FFT) of (e), which is the unnormalized *S*₂ spectra of graphene (red) and SiO₂ (black).

THz) are generated from a low-temperature-grown GaAs photoconductive antenna (PCA, TeTechS Inc.),²⁷ utilizing 35 fs 800 nm near-IR pulses from an 80 MHz Ti-sapphire oscillator. The collimated THz light is focused by a parabolic mirror (reflected focal length of 38.1 mm) onto the sample and AFM tip with $\sim 300 \mu\text{m}$ spot size. The tip-scattered THz light is directed and focused onto another PCA detector for coherent time-domain electric field detection. By changing the time delay of the 800 nm gate beam, the electric field of the

scattered THz pulse can be mapped to yield THz Time Domain Spectroscopy (THz-TDS).

To extract the near-field THz signal from the PCA receiver, the generated photocurrent is amplified with a low noise current preamplifier and demodulated by a lock-in amplifier at *n*th harmonics of the tip tapping frequency Ω to yield different orders of the scattered signal *S_n*. As shown in Figure 1c, THz-TDS signals *S*₁, *S*₂, and *S*₃ from a gold film can be obtained by demodulating the detected signal at first (Ω), second (2Ω),

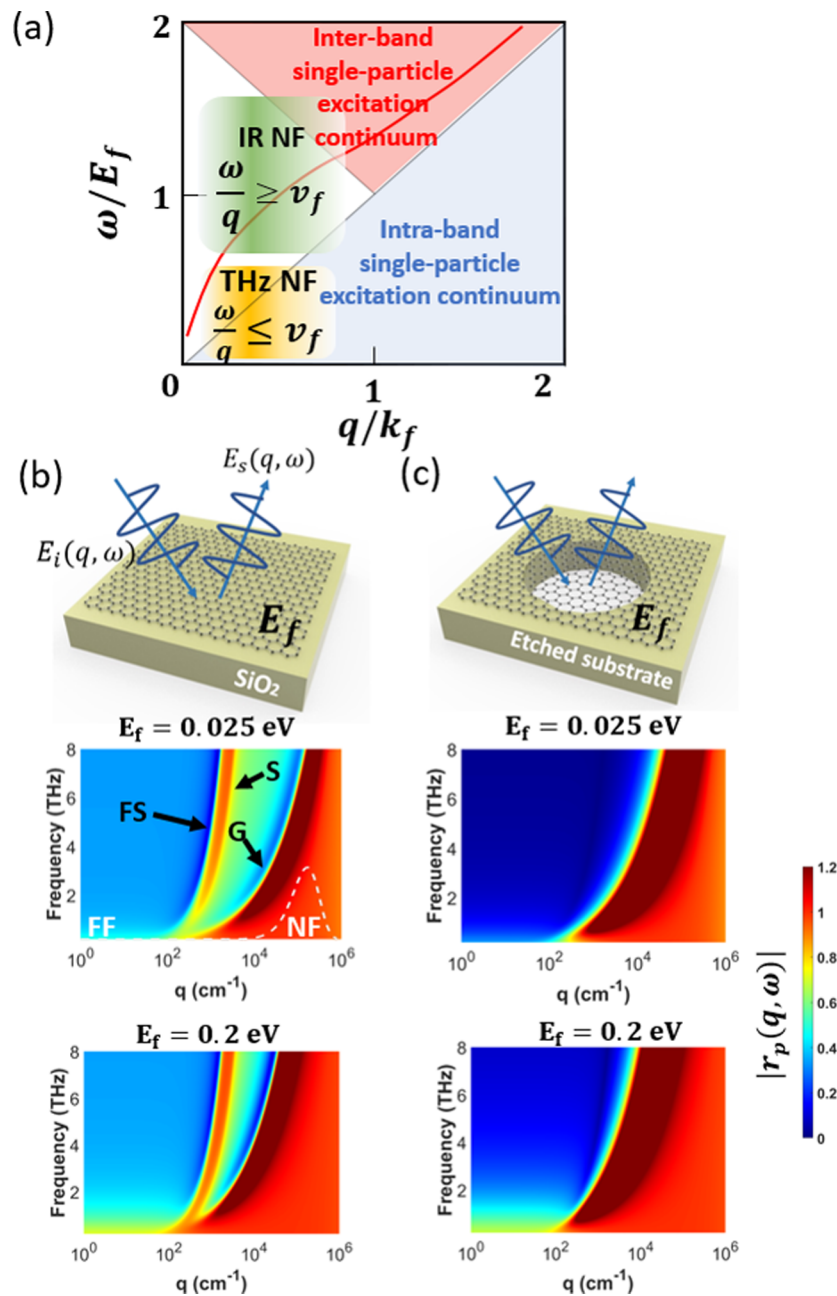


Figure 3. (a) Graphene dispersion adopted from Hwang et al.³⁵ Red curve denotes graphene plasmon dispersion; shaded green region indicates IR near-field accessible regime; shaded yellow region indicates THz near-field accessible regime. (b, c) Calculated $|\tau_p|$ of graphene at the THz range at room temperature using eqs 1–3. (b) Frequency-momentum dispersion of graphene/(300 nm) SiO_2 with $E_f = 0.025$ eV and $E_f = 0.2$ eV. The tip accessible high momentum region is indicated by the white dashed curve. FF: far-field region. NF: near-field region. FS: light line in free space. S: light line in SiO_2 . G: light line in supported graphene. Note the x axis is in log scale. (c) Frequency-momentum dispersion of freestanding graphene with $E_f = 0.025$ and 0.2 eV.

and third (3Ω) harmonics of the tip tapping frequency. With a ~ 80 μm long platinum tip (Rocky Mountain Nanotechnology), Ω is at ~ 20 kHz. We find that S_1 is approximately 3 orders of magnitude smaller than the incident far-field THz signal and is composed of both near-field and background signal that scattered from the AFM tip shank and cantilever. To yield genuine near-field signals with a spatial resolution < 100 nm, S_2 and S_3 should be used, which is a frequent practice in the s-SNOM community.^{28–30} We found S_2 is usually 3 to 10 times smaller than S_1 and S_3 2 to 3 times smaller than S_2 , using a typical 100–180 nm tip tapping amplitude. With a scan rate of 0.03 Hz/line and a lock-in time

constant of 100 ms, we can achieve a signal-to-noise ratio of more than 20 for S_2 . The spatial resolution is found to be below 100 nm. Before taking the near-field images, we maximize the peak of the near-field THz-TDS signal by adjusting the phase of the lock-in amplifier and the time delay. This ensures that we are plotting the spectral integrated peak THz electric field.

Using the THz near-field system, we performed nano-imaging of micrometer size graphene samples on SiO_2 (300 nm)/Si substrate. The graphene was mechanically exfoliated onto PDMS (Polydimethylsiloxane) and dry transferred onto a prepatterned Au lead (30 nm thick). Here the Au lead is used

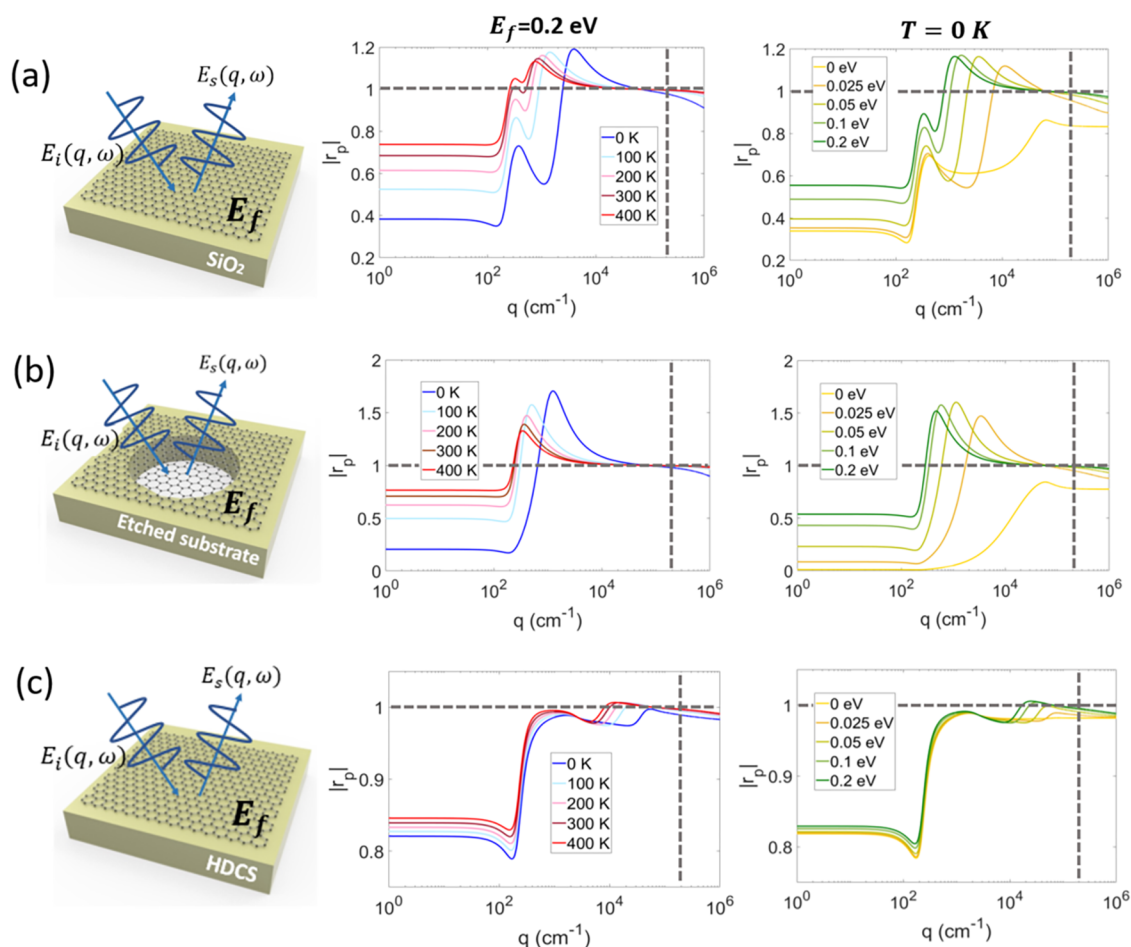


Figure 4. Calculation of the temperature and doping effects on graphene with different substrates: (a) SiO₂, (b) air, and (c) HDCS. Middle column displays temperature-dependent $|r_p|$ at 1 THz and $E_f = 0.2$ eV. Right column displays doping-dependent $|r_p|$ at 1 THz and $T = 0$ K. Gray dashed lines indicate where $|r_p| = 1$ (horizontal) and the dominant in-plane momentum $q = 2 \times 10^5$ cm⁻¹ (vertical), assuming a 50 nm tip apex.

for electrostatic gating and serves as a reference for graphene imaging. Figure 2a,b show the simultaneously collected AFM topography and near-field images with a size of 10×10 μm , respectively. As shown in Figure 2b, there is clearly a large optical contrast between single layer graphene (SLG, marked as 1) and the SiO₂ substrate (marked as 0). However, no obvious contrasts between SLG and multilayer graphene can be observed (the multilayers are marked by the number of layers as 2, 3, 4, and 5+). Moreover, a comparison between single-layer graphene and a 30 nm gold film revealed comparable THz near-field signals (see Figure 2c,d). These observations suggest that monolayer graphene has close-to-perfect near-field THz reflection.³¹ This near-unity THz near-field reflectivity is found to be independent of the carrier density when the back-gate voltage is swept between ± 30 V at room temperature (RT).

To compare the THz near-field spectra between SiO₂ and graphene, we plot the time domain signal in Figure 2e and the Fourier-transformed THz spectrum in Figure 2f. The normalized THz nanospectrum S_2 (graphene)/ S_2 (SiO₂) reveals that the near-field signal of graphene is 3–4 \times larger than that on the bare SiO₂ over the 0.2–1 THz frequency range. In the inset of Figure 2f, the unnormalized spectra of graphene and SiO₂ are plotted. A dip at about 0.75 THz can be observed, which was reported in previous THz near-field experiments.^{12,31} Since this dip is absent in the far-field THz

measurements using the same optics but excluding the involvement of the AFM tip (see Supporting Information), it is considered to be caused by the complex tip-light interactions and can be an interesting point for further investigation.

The THz s-SNOM image of graphene is clearly different from those taken at IR frequencies, in which graphene shows distinct near-field reflectivity depending on the layer thickness and stacking.²⁵ In the theoretical studies of far-field IR or THz properties of graphene, it is customary to consider the momentum-independent optical conductivity.^{32,33} In previous graphene near-field studies in the mid-infrared regime, the momentum-dependence (nonlocal effect) in the conductivity is usually ignored as well.^{22,24} This can be well justified by the fact that at IR frequencies, $\frac{\omega}{q} > v_f$, a local approximation ($\sigma(\omega, q) \approx \sigma(\omega, q = 0)$) can be applied. Here ω is the frequency of the incident light, v_f is the Fermi velocity, and q is the in-plane momentum of the scattered light, which can be on the order of $10^5 - 10^6$ cm⁻¹. However, in the THz regime, due to the low light frequency ω , $\frac{\omega}{q} \leq v_f$, the nonlocal effect is expected to be important and, therefore, shall be carefully addressed, as we will practice below.^{25,34} This “local” and “nonlocal” consideration of graphene is schematically demonstrated in Figure 3a, which illustrates the dispersion relation of graphene at moderate Fermi energy (~ 0.1 eV). As shown, a typical IR s-SNOM accesses an energy-momentum space

shaded by the green, while a typical THz s-SNOM accesses the space shaded by the yellow, which partially covers the intraband single particle continuum. The red solid curve displays graphene plasmon dispersion relation which, at IR frequencies, resides nominally in the “local” ($\frac{\omega}{q} > v_f$) regime.

To understand the high q near-field THz reflectivity, we employ the random phase approximation (RPA) approach, in which the frequency- (ω) and momentum- (q) dependent longitudinal optical conductivity of graphene is given by

$$\sigma(\omega, q) = \frac{ie^2\omega}{q^2}\Pi(\omega, q)$$

Π is the density–density response function.^{34,35} With RPA, the conductivity at zero temperature and zero electron interaction has been calculated to be

$$\sigma(\omega, q) = \sigma_0(\omega, q) \left[1 + f \left(\frac{\hbar(\omega + i\tau^{-1}) + 2E_f}{\hbar v_f q} \right) - f \left(\frac{\hbar(\omega + i\tau^{-1}) - 2E_f}{\hbar v_f q} \right) \right] - \frac{2i}{\pi} \frac{e^2\omega E_f}{(\hbar v_f q)^2} \quad (1)$$

where e is electron charge, $v_f = 10^6$ m/s, $k_F = \sqrt{\pi|n|}$ is the Fermi momentum, $E_f = \hbar v_f k_F$ is the Fermi energy, $\tau = 500$ fs is the phenomenological relaxation time, corresponding to a carrier mobility of 40000 cm²/(V s) at carrier density of 10¹² cm⁻², which is kept as a constant for the following calculation. Here we use a relatively high carrier mobility to emphasize the resonant features and their substrate and temperature dependence in Figures 3 and 4. With a more realistic τ value (50 fs), which corresponds to a carrier mobility of ~4000 cm²/(V s) with a carrier density of 10¹² cm⁻² (common for graphene on SiO₂) the main conclusion is not altered (see the Supporting Information, Figure S3). In graphene with significant lower mobility (e.g., 10 fs relaxation time), we found both in theory and in experiments that the THz near-field reflection can start to deviate from unity.

$$\sigma_0(\omega, q) = -i \frac{e^2}{4\hbar} \frac{\omega + i\tau^{-1}}{\sqrt{v_f^2 q^2 - (\omega + i\tau^{-1})^2}} \quad (2)$$

is the intrinsic graphene conductivity and f is defined as $f(x) = -\frac{1}{\pi}(x\sqrt{1-x^2} - \arccos(x))$. Although finite temperature effect is expected to be relatively small and has no impact on the qualitative features, for the purpose of rigorosity, we invoke the Maldaque identity^{34,36} and the temperature-dependent graphene conductivity at $T > 0$ can be written as the integral

$$\sigma(\omega, q; T, E_f) = \int_{-\infty}^{\infty} dE_f' \frac{\sigma(\omega, q; T = 0, E_f')}{4k_B T \cosh^2\left(\frac{E_f' - E_f}{2k_B T}\right)} \quad (3)$$

The most common approach to interpret near-field response is to employ an analytical model or a numerical simulation scheme.^{37–40} However, in this work it is sufficient to investigate graphene’s near-field response simply by calculating the momentum- and frequency-dependent reflection coefficient. In graphene, the p -polarized reflection coefficient r_p , which is defined as the ratio of the scattered electric field to

incident electric field per unit area, is given by the frequency and momentum dependent Fresnel equation⁴¹

$$r_p(q, \omega) = \frac{\varepsilon_2 k_1^z - \varepsilon_1 k_2^z + \left(\frac{4\pi k_1^z k_2^z \sigma}{\omega}\right)}{\varepsilon_2 k_1^z + \varepsilon_1 k_2^z + \left(\frac{4\pi k_1^z k_2^z \sigma}{\omega}\right)} \quad (4)$$

where ε_1 and ε_2 are the permittivity of air and the substrate, $k_i^z = \sqrt{\varepsilon_i \frac{\omega^2}{c^2} - q^2}$ is the out-of-plane momentum in air ($i = 1$) or in the substrate ($i = 2$), and q is the in-plane momentum, the same as defined above. When the absorption is not significant, or, in the graphene case, when it is far away from plasmon dispersion, $r_p(q, \omega)$ has a small imaginary part. Therefore, it is instructive and sufficient to look at the modulus of r_p .

Prior to the discussion of the $|r_p(q, \omega)|$ calculations, we stress that, in typical s-SNOM experiments, the accessible in-plane momentum is centered at $q \sim 1/a$, where a is the radius of curvature of the tip apex, which is typically ~ 10 to ~ 100 nm. More specifically, in a point-dipole approximation, the accessible q in a typical s-SNOM experiments follows a weight function given by $q^2 e^{-2qz_d}$,⁴¹ where z_d is the distance between tip apex and the sample.^{22,41,42} Assuming $a \approx 50$ nm, the time averaged weight function displays a “bell-shape”, which is drawn as white dashed curve in Figure 3b. Therefore, the most relevant q is in the order of 10⁵ cm⁻¹ to 10⁶ cm⁻¹, much larger than the momentum of the THz light in free space, which is about 10² cm⁻¹.^{41,42} For convenience, here we define $q > 10^5$ cm⁻¹ as the “high q ” regime, and $q < 10^2$ cm⁻¹ as the “low q ” regime.

Using eqs 1–4, $|r_p(q, \omega)|$ of graphene can be calculated at room temperature with different Fermi levels (e.g., $E_f = 0.025$ eV and $E_f = 0.2$ eV), as shown in Figure 3b (graphene on SiO₂) and Figure 3c (suspended graphene). In graphene on SiO₂, the low q (“far-field”) reflectivity $R = |r_p|^2$ is $\sim 20\%$, while the high q (“near-field”) reflection coefficient $|r_p| \approx 1$. Interestingly, in suspended graphene (Figure 3c), $|r_p|$ decreases dramatically at low q regime while remains close to unity at moderately high q . Based on Figure 3b,c, we conclude that at ambient environment (with an extrinsic random doping at level of ~ 0.025 eV), graphene can work as a near-perfect THz near-field reflector for s-SNOM.

The calculations of $r_p(q, \omega)$ is also performed when considering only the local conductivity $\sigma(\omega, q = 0)$, which is a common practice in the near-field study at infrared frequencies. The results are shown in Figure S1 in the Supporting Information. It is evident that the near-unity THz near-field reflection of graphene can be explained by the high- q reflectivity behavior (eq 4) without invoking the nonlocal conductivity. However, the local approximation slightly overestimates $r_p(q, \omega)$ in the high q regime. Therefore, for quantitative purpose, THz near-field calculations considering the nonlocal graphene conductivity is necessary, especially at low temperature and low doping where $r_p(q, \omega)$ starts to deviate from unity at high q values. We note that bare SiO₂ has a $|r_p|$ significantly less than 1 even with high q (see Supporting Information, Figure S1(c)). Consequently, SiO₂ exhibits a much lower THz near-field signal as observed in the experiments. Not surprisingly, gold films shows reflection coefficient close to one throughout the frequency-momentum space (Figure S1(d)). We also note that in the calculation of $|r_p|$, certain regions can have values above one (dark red). This

can be understood intuitively since for evanescent wave the out-of-plane component of light momentum is imaginary, and light is highly confined. Electric field is therefore strongly enhanced, leading to a local energy density that can be larger than that of the incident beam.

Next, we demonstrate the temperature and doping dependence of the graphene THz near-field response. In Figure 4, we plot the $|r_p(q, \omega = 1 \text{ THz})|$ as a function of q for graphene on different substrates: (a) SiO₂, (b) air, and (c) high dielectric constant substrate (HDCS) with a dispersionless $\epsilon = 100$. On all substrates, $|r_p(q, \omega = 1 \text{ THz})|$ is very close to unity in the high q regime from RT down to zero temperature, with a doping level at $E_f = 0.2 \text{ eV}$. At zero temperature, $|r_p(q, \omega = 1 \text{ THz})|$ in the high q regime is only slightly below unity, with the exception for intrinsic (undoped) graphene, where the r_p is around $\sim 80\%$ at high q . Since graphene on SiO₂ is known to be randomly doped by the substrate^{43,44} to ~ 0.1 to 0.2 eV , this deviation from unity may be hard to observe experimentally in high mobility graphene with gating. The temperature dependence of $|r_p(q, \omega)|$ may also be smeared out in experiments, especially if the sample has a smaller relaxation time τ (a larger Drude peak width).

In conclusion, we have carried out THz s-SNOM measurements on graphene/SiO₂ at 0.2–1 THz range with $<100 \text{ nm}$ spatial resolution. Our results show that graphene has a high near-field reflectivity that is comparable to gold thin films. We also demonstrate that the doping level, substrate dielectrics, and temperature have an insignificant effect on the high q response of graphene. The only exception for high mobility graphene, as suggested by our calculation using nonlocal optical conductivity, lies in extreme cryogenic condition. The near-unity response results from the unique dielectric properties of graphene and the nature of high momentum optics. Since graphene can be easily made, deformed or transferred onto different surfaces or structures, and most importantly, unlike thick noble metals, graphene does not add edge artifact, it can work as an ideal reference in the future for THz near-field experiments.

■ ASSOCIATED CONTENT

Supporting Information

The Supporting Information is available free of charge on the ACS Publications website at DOI: 10.1021/acsp Photonics.8b00190.

Experimental details and supporting figures and references (PDF).

■ AUTHOR INFORMATION

Corresponding Author

*E-mail: mengkun.liu@stonybrook.edu.

ORCID

Jiawei Zhang: 0000-0002-6135-1571

Xu Du: 0000-0001-5610-2338

Author Contributions

[‡]These authors contributed equally.

Notes

The authors declare no competing financial interest.

■ ACKNOWLEDGMENTS

M.K.L. acknowledges the helpful discussion with H. T. (Ted) Stinson, Michael M. Fogler, D. N. Basov, and Andreas Huber

(Neaspec) and important technical support from ITHATRON NANO-optics, NT-MDT, and TeTechS. This work is partially supported by the National Science Foundation under the CMMI Division (Grant Nos. 1563422 and 1562915). H. L. acknowledges the “Hundred-Talent” Program of Chinese Academy of Sciences and the National Natural Science Foundation of China (61575214).

■ REFERENCES

- (1) Sun, Y.; Sy, M. Y.; Wang, Y.-X. J.; Ahuja, A. T.; Zhang, Y.-T.; Pickwell-Macpherson, E. A Promising Diagnostic Method: Terahertz Pulsed Imaging and Spectroscopy. *World J. Radiol.* **2011**, *3* (3), 55.
- (2) Grossman, E.; Dietlein, C.; Ala-Laurinaho, J.; Leivo, M.; Gronberg, L.; Gronholm, M.; Lappalainen, P.; Rautiainen, A.; Tamminen, A.; Luukanen, A. Passive Terahertz Camera for Standoff Security Screening. *Appl. Opt.* **2010**, *49* (19), E106.
- (3) Nagatsuma, T.; Ducournau, G.; Renaud, C. C. Advances in Terahertz Communications Accelerated by Photonics. *Nat. Photonics* **2016**, *10* (6), 371–379.
- (4) Markelz, A. G.; Roitberg, A.; Heilweil, E. J. Pulsed Terahertz Spectroscopy of DNA, Bovine Serum Albumin and Collagen between 0.1 and 2.0 THz. *Chem. Phys. Lett.* **2000**, *320* (1–2), 42–48.
- (5) Markelz, A.; Whitmire, S.; Hillebrecht, J.; Birge, R. THz Time Domain Spectroscopy of Biomolecular Conformational Modes. *Phys. Med. Biol.* **2002**, *47* (21), 3797–3805.
- (6) Zhou, Z.; Zhou, T.; Zhang, S.; Shi, Z.; Chen, Y.; Wan, W.; Li, X.; Chen, X.; Gilbert Corder, S. N.; Fu, Z.; et al. Multicolor T-Ray Imaging Using Multispectral Metamaterials. *Adv. Sci.* **2018**, 1700982.
- (7) Nakanishi, H.; Fujiwara, S.; Takayama, K.; Kawayama, I.; Murakami, H.; Tonouchi, M. Imaging of a Polycrystalline Silicon Solar Cell Using a Laser Terahertz Emission Microscope. *Appl. Phys. Express* **2012**, *5* (11), 112301.
- (8) Jepsen, P. U.; Cooke, D. G.; Koch, M. Terahertz Spectroscopy and Imaging - Modern Techniques and Applications. *Laser Photonics Rev.* **2011**, *5* (1), 124–166.
- (9) Suzuki, D.; Oda, S.; Kawano, Y. A Flexible and Wearable Terahertz Scanner. *Nat. Photonics* **2016**, *10* (12), 809–813.
- (10) Huber, A. J.; Keilmann, F.; Wittborn, J.; Aizpurua, J.; Hillenbrand, R. Terahertz near-Field Nanoscopy of Mobile Carriers in Single Semiconductor Nanodevices. *Nano Lett.* **2008**, *8* (11), 3766–3770.
- (11) Liewald, C.; Mastel, S.; Hesler, J.; Huber, A. J.; Hillenbrand, R.; Keilmann, F. All-Electronic Terahertz Nanoscopy. *Optica* **2018**, *5* (2), 159.
- (12) Stinson, H. T.; Sternbach, A.; Najera, O.; Jing, R.; Mcleod, A. S.; Shusar, T. V.; Mueller, A.; Anderegg, L.; Kim, H. T.; Rozenberg, M. Imaging the Nanoscale Phase Separation in Vanadium Dioxide Thin Films at Terahertz Frequencies. *arXiv:1711.05242 [cond-mat.mes-hall]*, **2017**.
- (13) Kuschewski, F.; Von Ribbeck, H. G.; Döring, J.; Winnerl, S.; Eng, L. M.; Kehr, S. C. Narrow-Band near-Field Nanoscopy in the Spectral Range from 1.3 to 8.5 THz. *Appl. Phys. Lett.* **2016**, *108* (11), 113102.
- (14) Hasan, M.; Arezoomandan, S.; Condori, H.; Sensale-Rodriguez, B. Graphene Terahertz Devices for Communications Applications. *Nano Commun. Netw.* **2016**, *10*, 68–78.
- (15) Tassin, P.; Koschny, T.; Soukoulis, C. M. Graphene for Terahertz Applications. *Science* **2013**, *341*, 620–621.
- (16) Sensale-Rodriguez, B.; Yan, R.; Kelly, M. M.; Fang, T.; Tahy, K.; Hwang, W. S.; Jena, D.; Liu, L.; Xing, H. G. Broadband Graphene Terahertz Modulators Enabled by Intraband Transitions. *Nat. Commun.* **2012**, *3*, 780.
- (17) Palacios, T.; Hsu, A.; Wang, H. Applications of Graphene Devices in RF Communications. *IEEE Commun. Mag.* **2010**, *48* (6), 122–128.
- (18) Mueller, T.; Xia, F.; Avouris, P. Graphene Photodetectors for High-Speed Optical Communications. *Nat. Photonics* **2010**, *4* (5), 297–301.

- (19) Mittendorff, M.; Li, S.; Murphy, T. E. Graphene-Based Waveguide-Integrated Terahertz Modulator. *ACS Photonics* **2017**, *4* (2), 316–321.
- (20) Zhao, C. X.; Xu, W.; Li, L. L.; Zhang, C.; Peeters, F. M. Terahertz Plasmon-Polariton Modes in Graphene Driven by Electric Field inside a Fabry-Pérot Cavity. *J. Appl. Phys.* **2015**, *117* (22), 223104.
- (21) Gu, X.; Lin, I. T.; Liu, J. M. Extremely Confined Terahertz Surface Plasmon-Polaritons in Graphene-Metal Structures. *Appl. Phys. Lett.* **2013**, *103* (7), 071103.
- (22) Fei, Z.; Rodin, A. S.; Andreev, G. O.; Bao, W.; McLeod, A. S.; Wagner, M.; Zhang, L. M.; Zhao, Z.; Thiemens, M.; Dominguez, G.; et al. Gate-Tuning of Graphene Plasmons Revealed by Infrared Nano-Imaging. *Nature* **2012**, *487* (7405), 82–85.
- (23) Nikitin, A. Y.; Guinea, F.; García-Vidal, F. J.; Martín-Moreno, L. Edge and Waveguide Terahertz Surface Plasmon Modes in Graphene Microribbons. *Phys. Rev. B: Condens. Matter Mater. Phys.* **2011**, *84*, 161407.
- (24) Chen, J.; Badioli, M.; Alonso-González, P.; Thongrattanasiri, S.; Huth, F.; Osmond, J.; Spasenović, M.; Centeno, A.; Pesquera, A.; Godignon, P.; et al. Optical Nano-Imaging of Gate-Tunable Graphene Plasmons. *Nature* **2012**, *487* (7405), 77–81.
- (25) Kim, D.-S.; Kwon, H.; Nikitin, A. Y.; Ahn, S.; Martín-Moreno, L.; García-Vidal, F. J.; Ryu, S.; Min, H.; Kim, Z. H. Stacking Structures of Few-Layer Graphene Revealed by Phase-Sensitive Infrared Nanoscopy. *ACS Nano* **2015**, *9* (7), 6765–6773.
- (26) Honig, M.; Sulpizio, J. A.; Drori, J.; Joshua, A.; Zeldov, E.; Ilani, S. Local Electrostatic Imaging of Striped Domain Order in LaAlO₃/SrTiO₃. *Nat. Mater.* **2013**, *12*, 1112–1118.
- (27) Němec, H.; Pashkin, A.; Kužel, P.; Khazan, M.; Schüll, S.; Wilke, I. Carrier Dynamics in Low-Temperature Grown GaAs Studied by Terahertz Emission Spectroscopy. *J. Appl. Phys.* **2001**, *90* (3), 1303–1306.
- (28) Hillenbrand, R.; Keilmann, F. Material-Specific Mapping of Metal/semiconductor/dielectric Nanosystems at 10 Nm Resolution by Backscattering near-Field Optical Microscopy. *Appl. Phys. Lett.* **2002**, *80* (1), 25–27.
- (29) Hillenbrand, R.; Taubner, T.; Keilmann, F. Phonon-Enhanced Light-matter Interaction at the Nanometre Scale. *Nature* **2002**, *418* (6894), 159–162.
- (30) Qazilbash, M. M.; Brehm, M.; Chae, B.-G.; Ho, P.-C.; Andreev, G. O.; Kim, B.-J.; Yun, S. J.; Balatsky, A. V.; Maple, M. B.; Keilmann, F.; et al. Mott Transition in VO₂ Revealed by Infrared Spectroscopy and Nano-Imaging. *Science* **2007**, *318* (5857), 1750–1753.
- (31) Mastel, S.; Lundeberg, M. B.; Alonso-González, P.; Gao, Y.; Watanabe, K.; Taniguchi, T.; Hone, J.; Koppens, F. H. L.; Nikitin, A. Y.; Hillenbrand, R. Terahertz Nanofocusing with Cantilevered Terahertz-Resonant Antenna Tips. *Nano Lett.* **2017**, *17* (11), 6526–6533.
- (32) Andryieuski, A.; Lavrinenko, A. V. Graphene Metamaterials Based Tunable Terahertz Absorber: Effective Surface Conductivity Approach. *Opt. Express* **2013**, *21* (7), 9144.
- (33) Llatser, I.; Kremers, C.; Cabellos-Aparicio, A.; Jornet, J. M.; Alarcón, E.; Chigrin, D. N. Graphene-Based Nano-Patch Antenna for Terahertz Radiation. *Photonics Nanostructures - Fundam. Appl.* **2012**, *10* (4), 353–358.
- (34) Lundeberg, M. B.; Gao, Y.; Asgari, R.; Tan, C.; Duppen, B.; Van Autore, M.; Alonso-González, P.; Woessner, A.; Watanabe, K.; Taniguchi, T.; et al. Tuning Quantum Nonlocal Effects in Graphene Plasmonics. *Science* **2017**, *357* (6347), 187–191.
- (35) Hwang, E. H.; Das Sarma, S. Dielectric Function, Screening, and Plasmons in Two-Dimensional Graphene. *Phys. Rev. B: Condens. Matter Mater. Phys.* **2007**, *75* (20), 205418.
- (36) Giuliani, G.; Vignale, G. *Quantum Theory of the Electron Liquid*; Cambridge University Press, 2008.
- (37) Cvitkovic, A.; Ocelic, N.; Hillenbrand, R. Analytical Model for Quantitative Prediction of Material Contrasts in Scattering-Type near-Field Optical Microscopy. *Opt. Express* **2007**, *15* (14), 8550.
- (38) McLeod, A. S.; Kelly, P.; Goldflam, M. D.; Gainsforth, Z.; Westphal, A. J.; Dominguez, G.; Thiemens, M. H.; Fogler, M. M.; Basov, D. N. Model for Quantitative Tip-Enhanced Spectroscopy and the Extraction of Nanoscale-Resolved Optical Constants. *Phys. Rev. B: Condens. Matter Mater. Phys.* **2014**, *90* (8), 1–17.
- (39) Chui, S. T.; Chen, X.; Liu, M.; Lin, Z.; Zi, J. Scattering of Electromagnetic Waves from a Cone with Conformal Mapping: Application to Scanning near-Field Optical Microscope. *Phys. Rev. B: Condens. Matter Mater. Phys.* **2018**, *97* (8), 81406.
- (40) Chen, X.; Lo, C. F. B.; Zheng, W.; Hu, H.; Dai, Q.; Liu, M. Rigorous Numerical Modeling of Scattering-Type Scanning near-Field Optical Microscopy and Spectroscopy. *Appl. Phys. Lett.* **2017**, *111* (22), 223110.
- (41) Fei, Z.; Andreev, G. O.; Bao, W.; Zhang, L. M.; S. McLeod, A.; Wang, C.; Stewart, M. K.; Zhao, Z.; Dominguez, G.; Thiemens, M.; et al. Infrared Nanoscopy of Dirac Plasmons at the Graphene-SiO₂ Interface. *Nano Lett.* **2011**, *11*, 4701–4705.
- (42) Dai, S.; Fei, Z.; Ma, Q.; Rodin, A. S.; Wagner, M.; McLeod, A. S.; Liu, M. K.; Gannett, W.; Regan, W.; Watanabe, K.; et al. Tunable Phonon Polaritons in Atomically Thin van Der Waals Crystals of Boron Nitride. *Science* **2014**, *343* (6175), 1125–1129.
- (43) Berciaud, S.; Ryu, S.; Brus, L. E.; Heinz, T. F. Probing the Intrinsic Properties of Exfoliated Graphene: Raman Spectroscopy of Free-Standing Monolayers. *Nano Lett.* **2009**, *9* (1), 346–352.
- (44) Ryu, S.; Liu, L.; Berciaud, S.; Yu, Y. J.; Liu, H.; Kim, P.; Flynn, G. W.; Brus, L. E. Atmospheric Oxygen Binding and Hole Doping in Deformed Graphene on a SiO₂ Substrate. *Nano Lett.* **2010**, *10* (12), 4944–4951.